Testing Self-Similarity Through Lamperti Transformations

Myoungji LEE, Marc G. GENTON, and Mikyoung JUN

Self-similar processes have been widely used in modeling real-world phenomena occurring in environmetrics, network traffic, image processing, and stock pricing, to name but a few. The estimation of the degree of self-similarity has been studied extensively, while statistical tests for self-similarity are scarce and limited to processes indexed in one dimension. This paper proposes a statistical hypothesis test procedure for self-similarity of a stochastic process indexed in one dimension and multi-self-similarity for a random field indexed in higher dimensions. If self-similarity is not rejected, our test provides a set of estimated self-similarity indexes. The key is to test stationarity of the inverse Lamperti transformations of the process. The inverse Lamperti transformation of a self-similar process is a strongly stationary process, revealing a theoretical connection between the two processes. To demonstrate the capability of our test, we test self-similarity of fractional Brownian motions and sheets, their time deformations and mixtures with Gaussian white noise, and the generalized Cauchy family. We also apply the self-similarity test to real data: annual minimum water levels of the Nile River, network traffic records, and surface heights of food wrappings.

Key Words: Fractional Brownian sheet; Hurst coefficient; Hypothesis test; Multi-self-similarity; Random fields; Stationarity.

1. INTRODUCTION

A stochastic process is self-similar if it is invariant in distribution under suitable scaling of its index (Samorodnitsky and Taqqu 1994). Formally, a stochastic process, $\{X(\mathbf{t}),\ \mathbf{t} \in \mathbb{R}^d\}$ for $d \geq 1$, is said to be self-similar with index $H > 0$ (H-ss) if

$$\{X(a\mathbf{t}),\ \mathbf{t} \in \mathbb{R}^d\} \overset{\mathcal{L}}{=} \{a^H X(\mathbf{t}),\ \mathbf{t} \in \mathbb{R}^d\}, \tag{1}$$

for all $a > 0$, where $\overset{\mathcal{L}}{=}$ denotes equality of the finite dimensional distributions. A self-similar process behaves the same when viewed at different scales. Due to its ability to explain the

Myoungji Lee Institute for Applied Mathematics and Computational Science, Texas A&M University, College Station, TX 77843-3143, USA (E-mail: *myoungji@tamu.edu*). Marc G. Genton (✉) CEMSE Division, King Abdullah University of Science and Technology, Thuwal 23955-6900, Saudi Arabia (E-mail: *marc.genton@kaust.edu.sa*). Mikyoung Jun Department of Statistics, Texas A&M University, College Station, TX 77843-3143, USA (E-mail: *mjun@stat.tamu.edu*).

Journal of Agricultural, Biological, and Environmental Statistics, 21:426–447
DOI: 10.1007/s13253-016-0258-1

long-range dependence that persists in a process with a single parameter, H, self-similarity has been widely used in modeling various natural, environmental, physical, and biological phenomena, such as river water levels, network traffic, image processing, and stock pricing, to name but a few recent works (Ghanbarian-Alavijeh et al. 2011; Li and Zhao 2012; Bai and Shami 2013).

When a process is assumed to be self-similar, the estimation of its self-similarity index has been vastly studied over the last few decades. Although self-similarity is a strong assumption, namely the distributional invariance with respect to a proper scaling, there have been relatively few statistical hypothesis tests for the presence of self-similarity of a time series. Leland et al. (1994) constructed a new set of time series by averaging the original series over non-overlapping blocks of size $m = 1, \ldots, 1000$. Due to the scale invariance of self-similar processes, the estimated index stabilizes around the true index as m increases. They examined self-similarity graphically by plotting the variances of the aggregated processes, the rescaled adjusted range statistic, and the periodogram, all of which are commonly used statistics to estimate the self-similarity index. Bardet (2000) examined the difference between the observed and expected generalized quadratic variations under self-similarity. Hall et al. (2000) estimated the self-similarity index of stock prices by rescaled adjusted range analysis. Then they tested if the process is self-similar with index $H = 0.5$, which is important because stock prices have independent increments. Gneiting and Schlather (2003) estimated the measures of long-range and short-range dependence that are the Hurst coefficient, H, and the fractal dimension, D, respectively. They tested self-similarity by examining $H + D = d + 1$, which holds if the process is self-similar. Bianchi (2004) applied a Kolmogorov–Smirnov goodness-of-fit test to measure the equality of the distributions on both sides of (1). All these tests focused on testing if $\{X(\mathbf{t}), \mathbf{t} \in \mathbb{R}^d\}$ is H-ss for $0 < H \leq 1$ and $d = 1$.

We propose a new statistical hypothesis test for self-similarity of a stochastic process indexed in one or higher dimensions. Our approach is capable of detecting multi-self-similarity of a random field (Genton et al. 2007), a generalization of (1) under which the stochastic process has different degrees of self-similarity in each dimension. Our test is based on the Lamperti transformation that connects two important characteristics of stochastic processes, self-similarity and strong stationarity (see Lamperti (1962) for $d = 1$ and Genton et al. (2007) for $d \geq 1$). The Lamperti transformation of a strongly stationary process is self-similar, and the inverse Lamperti transformation of a self-similar process is strongly stationary. A strongly stationary process is a stochastic process Y that is invariant under translation, i.e., $\{Y(\mathbf{t} + \mathbf{h}),\ \mathbf{t} \in \mathbb{R}^d\} \stackrel{\mathcal{L}}{=} \{Y(\mathbf{t}),\ \mathbf{t} \in \mathbb{R}^d\}$, for all $\mathbf{h} \in \mathbb{R}^d$. Note that a stochastic process is weakly stationary if it has a constant mean and the covariance function, $C(\mathbf{x} - \mathbf{y}) = \operatorname{cov}\{Y(\mathbf{x}), Y(\mathbf{y})\}$, for all $\mathbf{x}$ and $\mathbf{y} \in \mathbb{R}^d$. All strongly stationary processes are weakly stationary, but the converse is not necessarily true. However, strong and weak stationarities are equivalent for Gaussian processes. Hereafter, we mean by stationarity the weak form of stationarity.

The mathematical relationships of various statistics, such as covariance functions and spectral densities of the original process and its Lamperti transformations, have been studied substantially (Flandrin et al. 2003). However, the Lamperti transformation has not been well exploited in the sense that one can use theories developed for stationary processes on self-similar processes, and vice versa. Due to the lack of testing methods for strong stationarity, we test self-similarity of a stochastic process by testing weak stationarity of its inverse Lamperti transformation, which is equivalent for Gaussian processes. Then we provide a set of the estimated self-similarity indexes that produce stationary transformations.

There is substantial literature on statistical hypothesis tests for stationarity of a time series and a few stationarity tests for a random field. Priestley and Subba Rao (1969) tested stationarity of a time series by examining uniformity of the logarithm of the evolutionary spectrums across time. Dwivedi and Subba Rao (2011) proposed a test for stationarity using the fact that the discrete Fourier transform is asymptotically uncorrelated at the canonical frequencies if and only if the time series is second-order stationary. Jentsch and Subba Rao (2015) extended the test by Dwivedi and Subba Rao (2011) to multivariate time series. Recently, Cardinali and Nason (2011) and Nason (2013) developed tests to detect the costationarity of two time series, under which a certain linear combination of the two series is stationary. Nason (2013) also aimed at detecting the locations at which non-stationarity occurs and compared the performance of his test to the stationarity test presented by Priestley and Subba Rao (1969). More stationarity tests can be found in the references therein.

Fuentes (2005) extended the test by Priestley and Subba Rao (1969) to gridded observations in two dimensions. Subba Rao (2008) developed a stationarity test in the spatial domain for spatiotemporal processes by considering an autoregressive model in time at each spatial location and comparing how the autoregressive coefficients differed by locations. Jun and Genton (2012) provided a non-parametric stationarity test for spatial and spatiotemporal multivariate random fields on a planar or spherical domain. They estimated the covariance at certain spatial and temporal lags and constructed a statistical hypothesis test based on the asymptotic normality of the estimated covariance under weak stationarity. All of these methods tested weak stationarity of a Gaussian process.

We use the stationarity tests presented by Priestley and Subba Rao (1969) and Fuentes (2005) for a stochastic process indexed in one and two dimensions, respectively. A primary reason of using these tests is their computational simplicity. Their p values are defined in a closed form without restrictions, while Nason (2013) requires the sample size to be a power of two and Jentsch and Subba Rao (2015) require bootstrap samplings to calculate p values. A secondary reason is for fair comparison of the performance of the multi-self-similarity test in one and two dimensions, as Fuentes (2005) extended the test by Priestley and Subba Rao (1969) to higher dimensions.

This paper is organized as follows. Section 2 describes the test procedures for multi-self-similarity. Section 3 studies the empirical sizes and powers of the multi-self-similarity test through fractional Brownian motions and sheets, their time deformations and mixtures with Gaussian white noise, and the generalized Cauchy family. Section 4 applies the multi-self-similarity test to annual minimum water levels of the Nile River, to records of Ethernet traffic amounts, and to surface heights of food wrappings. Section 5 summarizes the results and concludes with suggestions for possible future work.

2. TESTING AND ESTIMATING MULTI-SELF-SIMILARITY

Let $\mathbb{R}_+$ and $\mathbb{R}_+^d$ be the space of positive real values and the d-fold Cartesian product, $\mathbb{R}_+ \times \cdots \times \mathbb{R}_+$, respectively. A random field, $\{X(\mathbf{t}), \mathbf{t} = (t_1, \ldots, t_d)^T \in \mathbb{R}^d\}$ for $d \geq 1$, is multi-self-similar with index $\mathbf{H} = (H_1, \ldots, H_d)^T \in \mathbb{R}_+^d (\mathbf{H} - \text{mss})$ if

$$\{X(a_1 t_1, \ldots, a_d t_d),\ \mathbf{t} \in \mathbb{R}^d\} \overset{\mathcal{L}}{=} \{a_1^{H_1} \cdots a_d^{H_d} X(t_1, \ldots, t_d),\ \mathbf{t} \in \mathbb{R}^d\}, \tag{2}$$

for all $a_1, \ldots, a_d > 0$ (Genton et al. 2007, def. 2.1.1). If $a_1 = \cdots = a_n = a > 0$, then (2) reduces to (1) with $H_1 + \cdots + H_d = H > 0$. For every strongly stationary process, $\{Y(\mathbf{t}), \mathbf{t} \in \mathbb{R}^d\}$, its Lamperti transformation,

$$X_{\mathbf{H}}(\mathbf{t}) = t_1^{H_1} \cdots t_d^{H_d} Y(\log(t_1), \ldots, \log(t_d)), \quad \mathbf{t} \in \mathbb{R}_+^d,$$

is well defined and $\mathbf{H}$-mss. Conversely, if $\{X(\mathbf{t}), \mathbf{t} \in \mathbb{R}_+^d\}$ is $\mathbf{H}$-mss, then its inverse Lamperti transformation,

$$Y_{\mathbf{H}}(\mathbf{t}) = e^{-\mathbf{t}^T \mathbf{H}} X(e^{t_1}, \ldots, e^{t_d}), \quad \mathbf{t} \in \mathbb{R}^d, \tag{3}$$

is strongly stationary (Genton et al. 2007, prop. 2.1.1).

This paper focuses on the cases when $d = 1$ or 2, and $\mathbf{H} \in (0, 1]^d$. Most literature dealing with H-ss processes has been focused on the case when $H \in (0, 1]$. Also, it has been argued that H-ss processes with $H > 1$ are not of practical interest (Wang et al. 2001, p. 96). We therefore test multi-self-similarity of a random field, say X, when all components of the index, $\mathbf{H}$, are between 0 and 1. Hereafter, we call

$$X \text{ is } \mathbf{H}\text{-mss for some } \mathbf{H} \in (0, 1]^d,$$

the multi-self-similarity hypothesis (self-similarity hypothesis, if $d = 1$). Testing multi-self-similarity (self-similarity, if $d = 1$) of X consists of the hypothesis testing of

$$H_0 : X \text{ is } \mathbf{h}\text{-mss} \quad \text{vs} \quad H_a : X \text{ is not } \mathbf{h}\text{-mss}, \tag{4}$$

for each $\mathbf{h} \in \mathcal{H} = \{j/m, j = 1, \ldots, m\}^d \subset (0, 1]^d$, a finite set of indexes. We test the sufficient condition of H_0 in (4) by testing weak stationarity of the inverse Lamperti transformation, $Y_{\mathbf{h}}$ in (3). If the hypothesis test of (4) rejects the null hypothesis, H_0, for all $\mathbf{h} \in \mathcal{H}$ at significance level 0.05, we reject the multi-self-similarity hypothesis and conclude that X is not $\mathbf{h}$-mss for all $\mathbf{h} \in (0, 1]^d$. Otherwise, we conclude that X is multi-self-similar for some index in $(0, 1]^d$ and provide a set of estimated multi-self-similarity indexes associated with p values larger than 0.05. We reject the multi-self-similarity hypothesis if the maximum p value over all $\mathbf{h} \in \mathcal{H}$ is attained for $\mathbf{h}$ on the boundary of $\mathcal{H}$, such as $\mathbf{h} = (1, \ldots, 1)^T/m$. The set of the estimated indexes consists of contiguous values of $\mathbf{h}$ in all simulation studies and real data analyses presented in this paper. We therefore provide the center and the length or diameter of the set of the estimated indexes in one or two dimensions, respectively.

The fact that non-rejection of (4) occurs for consecutive values of $\mathbf{h}$ is the reason why a familywise error rate is not considered when testing (4) for multiple values of $\mathbf{h}$. Empirical

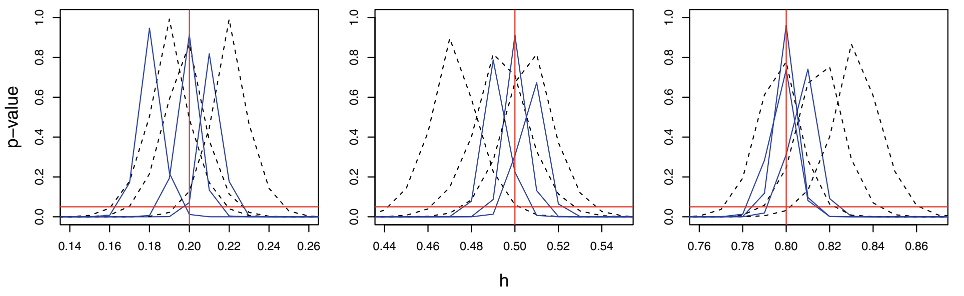

Figure 1. In six realizations of fractional Brownian motions with index 0.2 (*left*), 0.5 (*middle*), and 0.8 (*right*) observed on exponential index spacing, the p values of the hypothesis test of (4) are shown as *black dashed* and *blue solid lines* for sample sizes of 64 and 128, respectively. The *red lines* represent the true self-similarity index and the nominal significance level, 0.05 (Color figure online).

studies show that the p value of the test (4) as a function of $\mathbf{h}$ has one peak near the true $\mathbf{h}$, as in Figs. 1 and 4. These suggest that the chance of having false positives is very low, when $\mathbf{h}$ is away from the truth. This is due to extremely low p values produced for false $\mathbf{h}$, which indicate sensitivity of the Lamperti transformation on $\mathbf{h}$, i.e., the stationarity of the inverse Lamperti transformation, $Y_{\mathbf{h}}$, of a $\mathbf{H}$-mss process, does not hold if $\mathbf{h}$ is slightly different from $\mathbf{H}$.

For the choice m, we tried $m = 20$ and 100 in this paper and found them sufficient for one and two dimensions. For low dimensions, a bounded set, $(0, 1]^d$, is fine with grid search, although there could be a curse of dimensionality for high dimensions.

One important aspect of the Lamperti transformation is that it bridges a stationary process observed on a regular grid and a self-similar process observed on exponential index spacing. All of the stationarity tests indexed in one dimension and most stationarity tests indexed in two dimensions introduced in Sect. 1 are developed for a process observed regularly on its domain. Therefore, in order to apply the multi-self-similarity test, we are required to observe the process on exponential index spacing, while we observe a process on a regular grid in most real applications. To tackle this, we sample the process on an exponential scale multiple times. Then, we have multiple processes of shorter length, instead of one realization of a larger size. We perform the multi-self-similarity test to each subsequence and report the percentage of the subsequences that reject self-similarity. To ensure independence between subsequences, Pearson correlation coefficients of the subsequences were calculated for some simulation studies and real applications in Sects. 3 and 4. The correlations were centered between 0 and 0.3 with standard deviation around 0.25. As strong correlation among the subsequences can damage the efficiency of the proposed test, checking correlations is recommended before conducting the test.

More specifically, suppose that we observe $\{X(\mathbf{t}),\ \mathbf{t} \in \mathbb{Z}^d\}$. We consider the following subsequence of X:

$$\{X([e^{i_1+m}], \ldots, [e^{i_d+m}]),\ i_1 \in \Delta_1\mathbb{Z}, \ldots, i_d \in \Delta_d\mathbb{Z}\},$$

for some $\Delta_1, \ldots, \Delta_d > 0$ and $m \in \mathbb{R}$, where $[x]$ denotes the nearest integer of $x \in \mathbb{R}$. The numbers, $\Delta_1, \ldots, \Delta_d$, control the length of the subsequence. That is, a bigger Δ corresponds to shorter subsequences. To overcome the reduction in sample size, we take several such subsequences by varying m. For $\mathbf{h} = (h_1, \dots, h_d)^T \in (0, 1]^d$, let

$$Y_{\mathbf{h}}(i_1 + m, \dots, i_d + m) = e^{-(i_1+m)h_1 - \cdots - (i_d+m)h_d} X([e^{i_1+m}], \dots, [e^{i_d+m}])$$

and $\widetilde{Y}_{\mathbf{h}}(j_1, \dots, j_d) = Y_{\mathbf{h}}(\Delta_1 j_1 + m, \dots, \Delta_d j_d + m)$ for $\mathbf{j} = (j_1, \dots, j_d)^T \in \mathbb{Z}^d$. Then, $\widetilde{Y}_{\mathbf{h}}$ is indexed in $\mathbb{Z}^d$, and it is stationary if and only if $Y_{\mathbf{h}}$ is stationary. We test stationarity of $\widetilde{Y}_{\mathbf{h}}$ for $\mathbf{h} \in \mathcal{H}$, by the tests of Priestley and Subba Rao (1969) and Fuentes (2005). Both tests evaluate the evolutionary spectral density function for several locations and frequencies, which are asymptotically uncorrelated if the frequencies or the locations are sufficiently away from each other. Then, the uniformity of the logarithm of the evolutionary spectrum across location is tested by a two-way analysis of variance. In Sects. 3 and 4, we divide a time series into two subsequences of equal length and compare the evolutionary spectrum at the center points. Similarly, in two dimensions, we divide the domain of a random field into quadrangles of equal size and compare the spectrums at the centers of the two diagonal quadrangles. Implementations of the test procedures are provided in the Appendix. When $d = 1$, we use the function `stationarity` in the R library *fractal* that uses multiple sinusoidal tapers for a spectral density function.

3. MONTE CARLO SIMULATIONS

3.1. STOCHASTIC PROCESS INDEXED IN ONE DIMENSION ON EXPONENTIAL INDEX SPACING

A fractional Brownian motion with index $0 < H \leq 1$ is a unique Gaussian process that is H-ss and has stationary increments. It is mean zero and satisfies

$$\mathrm{E}\{X_H(t)X_H(s)\} = \frac{1}{2}\{|t|^{2H} + |s|^{2H} - |t - s|^{2H}\},$$

for all t and $s \in \mathbb{R}$. We first simulate fractional Brownian motions with index $H = 0.2, 0.5$, and 0.8 at $\{t = e^i,\ i = 1, \dots, 32\}$, $\{t = e^{i/2},\ i = 1, \dots, 64\}$, and $\{t = e^{i/4},\ i = 1, \dots, 128\}$. Since exactly simulating the fractional Brownian motion at $\{t = e^1, \dots, e^n\}$ is impossible for $n = 64$ and 128 for numerical reasons, the process is simulated on the exponential of fractions when sample size, n, is 64 and 128. Throughout Sect. 3.1, we test (4) for $h \in \mathcal{H} = \{j/100,\ j = 1, \dots, 100\}$ to test self-similarity of a stochastic process. Figure 1 shows the p values of the hypothesis test of (4) for $h \in \mathcal{H}$, for six realizations of the fractional Brownian motion with index $H = 0.2, 0.5$, and 0.8, from left to right. The p values are from the stationarity test (Priestley and Subba Rao 1969) of Y_h for $h \in \mathcal{H}$. The p values are the highest around the true self-similarity index and decrease as h becomes distant from the true index, to less than 10^{-30}. The larger the sample size, the narrower the interval of h that produces p value larger than 0.05, and the more intervals include the true index from repeated simulations.

The self-similarity hypothesis is never rejected for all realizations of fractional Brownian motions, for all n and H, i.e., for each sample path of fractional Brownian motion, there is

Table 1. Out of 500 fractional Brownian motions with index H observed at n locations of exponential index spacing, empirical sizes (%) of the test of (4) for $h = H$ are listed along with the average centers and the average lengths of the estimated intervals in the parentheses.

	n	H		
		0.2	0.5	0.8
Empirical size (center, length)	32	7.2 (.201, .083)	10.0 (.500, .083)	14.0 (.798, .083)
	64	6.6 (.200, .058)	8.4 (.499, .058)	9.6 (.801, .059)
	128	4.8 (.199, .036)	4.8 (.500, .037)	8.2 (.799, .037)

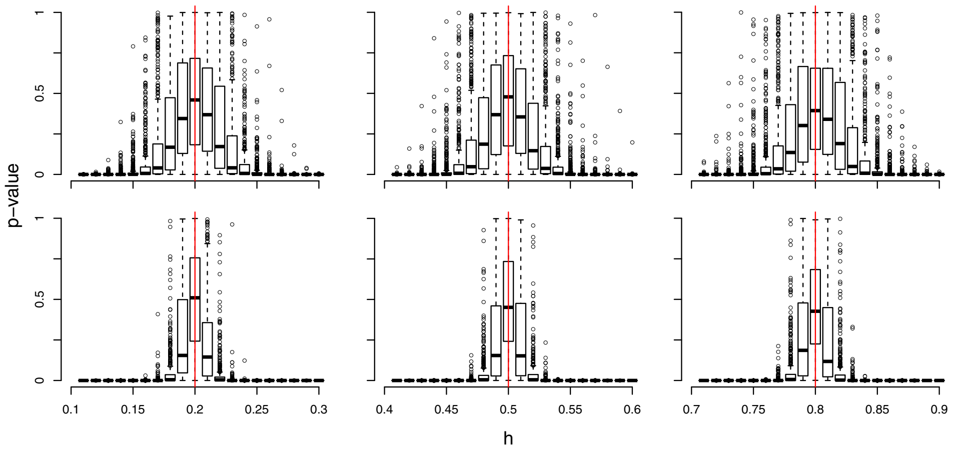

Figure 2. From *left* to *right*, the boxplots of the p values of the hypothesis test of (4) are shown for $h \in \mathcal{H}$, from 500 fractional Brownian motions with index 0.2, 0.5, and 0.8, respectively, observed at 64 (*upper*) and 128 (*lower*) locations of exponential index spacing.

at least one element of $\mathcal{H}$ that does not reject the hypothesis test of (4) at significance level 0.05. However, the test of (4) for $h = H$ is rejected for some realizations, due to the type I error of the stationarity test. Table 1 shows the empirical sizes (%) of the hypothesis test of (4) for $h = H$, i.e., the percentages of the cases in which the intervals of the estimated self-similarity indexes exclude the true index. They decrease to around the significance level, 5%, as n increases for $H = 0.2$ and 0.5. In the parentheses, the average centers and the average lengths of the estimated intervals are listed by sample size and self-similarity index. The intervals become narrow and centered near the true index as the sample size increases. Figure 2 shows the distributions of the p values of the hypothesis test of (4) by h. From left to right, the boxplots of the p values are shown for $H = 0.2, 0.5$, and 0.8, and the upper and bottom panels are for $n = 64$ and 128, respectively. The p values of the stationarity test for Y_H are nearly uniformly distributed over [0, 1], in accordance with the empirical sizes presented in Table 1.

Secondly, we simulate the stationary processes listed in Table 2, $\{Y(t),\ t = 1, \ldots, n\}$, for $n = 32$, 64, and 128, for 500 times, then we take its Lamperti transformation, $X(e^t) = e^{tH} Y(t)$, with $H = 0.2, 0.5$, or 0.8, to simulate self-similar processes with index H. Nason (2013) compared the empirical sizes of these stationary processes for several stationarity

Table 2. Stationary processes considered by Nason (2013).

Model 1:	Independent and identically distributed (iid) standard normal;
Model 2:	AR(1), with AR parameter of 0.9 and standard normal innovations;
Model 3:	AR(1) with parameter −0.9;
Model 4:	MA(1) with parameter 0.8;
Model 5:	MA(1) with parameter −0.8;
Model 6:	ARMA(1, 2) with AR parameter −0.4 and MA parameters of (−0.8, 0.4);
Model 7:	AR(2) with AR parameters $\alpha_1 = 1.385929$, and $\alpha_2 = -0.9604$, the case that is stationary but close to unit root.

The terms AR(p), MA(q) and ARMA(p, q) stand for an autoregressive model with order p, a moving-average model with order q, and an autoregressive moving-average model with order (p, q), respectively.

Table 3. Self-similarity test for the Lamperti transformation, $X(e^t) = e^{0.8t} Y(t), t = 1, \ldots, n$, of the stationary models, Y, in Table 2.

	n	Model						
		1	2	3	4	5	6	7
Empirical size (%)	32	7.0	18.2	7.6	6.6	7.0	11.2	11.4
	64	5.0	13.8	5.6	5.8	7.0	8.6	16.6
	128	4.6	5.4	3.0	5.8	5.2	3.8	7.4
(center, length)	32				(0.80, 0.08)			
	64				(0.80, 0.03)			
	128				(0.80, 0.01)			

The top half displays the empirical sizes (%) of the test of (4) for $h = 0.8$, and the bottom half displays the average centers and the average lengths of the intervals of the estimated self-similarity indexes from 500 repetitions.

tests, including the test by Priestley and Subba Rao (1969). When $n = 32$ and 64, the self-similarity hypothesis of X is never rejected for all stationary models and H. When $n = 128$, for each stationary model and H, the self-similarity hypothesis is rejected from 2 to 5 % out of 500 simulations. Table 3 shows the percentages of the cases in which the intervals of the estimated self-similarity indexes exclude the true index [empirical sizes (%) of the test of (4) for $h = H$] and the average centers and the average lengths of the estimated intervals, when $H = 0.8$. The results are similar when $H = 0.2$ or 0.5. Models 2 and 7 have large type I errors of the hypothesis test of (4) for $h = 0.8$, as reported by Nason (2013).

To study the empirical power, we simulate non-self-similar processes: time-deformed fractional Brownian motions and mean zero Gaussian processes with isotropic Matérn covariance. For a fractional Brownian motion with index H, X_H, the time-deformed fractional Brownian motion is defined as $X_H(M(t))$ for an increasing function, $M(t)$, for $t \in \mathbb{R}$. The functions $M(t)$ used in the simulations are listed in Table 4. The isotropic Matérn covariance function is

$$K(r; \sigma^2, \phi, \nu) = \sigma^2 \frac{(r/\phi)^\nu \mathcal{K}_\nu(r/\phi)}{2^{\nu-1}\Gamma(\nu)}, \tag{5}$$

for $r \geq 0$, where $\Gamma(z)$ is the gamma function and $\mathcal{K}_\nu$ is a Bessel function of the second kind of order ν. The parameters of the Matérn covariance function are the partial sill, $\sigma^2 > 0$, the range, $\phi > 0$, and the smoothness parameter, $\nu > 0$. A mean zero Gaussian process with (5)

Table 4. The empirical powers (%) of the self-similarity test for time-deformed fractional Brownian motions, $X_H(M(t))$, and mean zero Gaussian processes with Matérn covariance with parameters (σ^2, ϕ, ν), observed at n locations of exponential index spacing, from 500 repetitions.

	$M(t)$	n	H		
			0.2	0.5	0.8
1.	$\frac{t}{1000+t}$	32	99	100	100
		64	100	100	100
		128	100	100	100
2.	$\log(t+1)$	32	71	56	41
		64	82	79	60
		128	92	91	78
3.	$\log(t+100)$	32	66	49	30
		64	69	56	31
		128	82	63	48
4.	$\frac{\log(t+1)}{1+\log(t+1)}$	32	90	79	48
		64	99	98	87
		128	100	100	100
5.	$\frac{\log(t+100)}{1+\log(t+100)}$	32	85	68	41
		64	96	88	60
		128	100	100	79
6.	Matérn(1, 10, H)	32	78	77	81
		64	86	88	85
		128	94	93	91
7.	Matérn(1, 1000, H)	32	73	73	72
		64	84	78	69
		128	88	66	58

is locally self-similar with self-similarity index ν, if the process is mean square continuous but not differentiable, i.e., $0 < \nu < 1$ (Kent and Wood 1997; Stein 1999; Gneiting et al. 2012). A locally self-similar process with index $\nu \in (0, 1)$, Z, satisfies

$$\mathrm{cov}\{Z(t), Z(t+s)\} = \mathrm{var}\{Z(t)\} - A|s|^{2\nu} + o(|s|^{2\nu}), \quad \text{as} \quad |s| \to 0, \tag{6}$$

for all t and $s \in \mathbb{R}$ and for some $A > 0$. Note that the fractional Brownian motion with index $\nu \in (0, 1)$, X_ν, satisfies

$$\mathrm{cov}\{X_\nu(t), X_\nu(t+s)\} = \frac{\mathrm{var}\{X_\nu(t)\} + \mathrm{var}\{X_\nu(t+s)\}}{2} - \frac{1}{2}|s|^{2\nu},$$

for all t and $s \in \mathbb{R}$. Figure 3 plots a Brownian motion trajectory and non-self-similar processes listed in Table 4. A Brownian motion is a fractional Brownian motion with index 0.5. Table 4 lists the percentages of the realizations that reject the self-similarity hypothesis out of 500 realizations at $\{t = e^i,\ i = 1, \ldots, 32\}$, $\{t = e^{i/2},\ i = 1, \ldots, 64\}$, and $\{t = e^{i/4},\ i = 1, \ldots, 128\}$; the cases when the p values of the hypothesis test of (4) are less than 0.05 for all $h \in \mathcal{H}$ or the cases when the p value is the maximum at $h = 0.01$, at the boundary of $\mathcal{H}$. In many realizations of a non-self-similar process, the p values of the

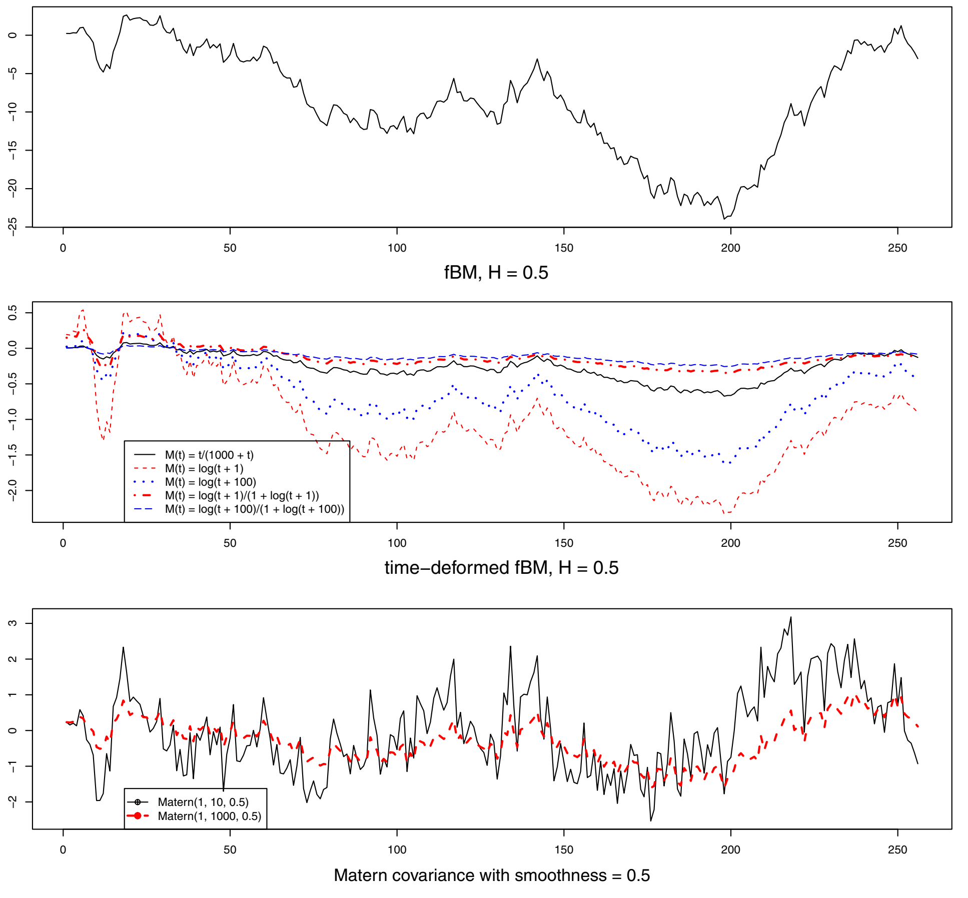

Figure 3. From the *top*, a sample path of Brownian motion, $\{X_{0.5}(t),\ t = 1, \ldots, 256\}$, its time deformations, $\{X_{0.5}(M(t))\}$, and Gaussian processes with Matérn covariance with smoothness $= 0.5$ are shown for $M(t)$ and the covariance parameters in Table 4.

hypothesis test of (4) are less than 0.05 for all $h \in \mathcal{H}$. For non-zero p values, there is often no upward and downward tendency as h increases, as seen in Fig. 1. Even if there exists such a pattern in the p values, the maximum p value is often smaller than 0.05. Generally, in Table 4, the larger the sample size, the higher the rejection rate. Also the large difference between the differential of M and 1, $|M'(t) - 1|$, is associated with the high rejection rate. This agrees with the fact that the differential is related to the degree of deformation. When the self-similarity hypothesis is not rejected, the average centers and the average lengths of the intervals of the estimated self-similarity indexes are less than 0.10 and 0.09, respectively, for all the processes and for all n and H.

For a non-self-similar process, we also study a mixture of fractional Brownian motion with index $H = 0.2, 0.5$, and 0.8, and Gaussian white noise, $\{X_H(t) + C\epsilon(t)\}$ simulated at $\{t = e^i,\ i = 1, \ldots, 32\}$, $\{t = e^{i/2},\ i = 1, \ldots, 64\}$, and $\{t = e^{i/4},\ i = 1, \ldots, 128\}$. The Gaussian white noise, $\epsilon(t)$, is independent and identically distributed (iid) standard normal random variables for all t. The self-similarity hypothesis is never rejected for all

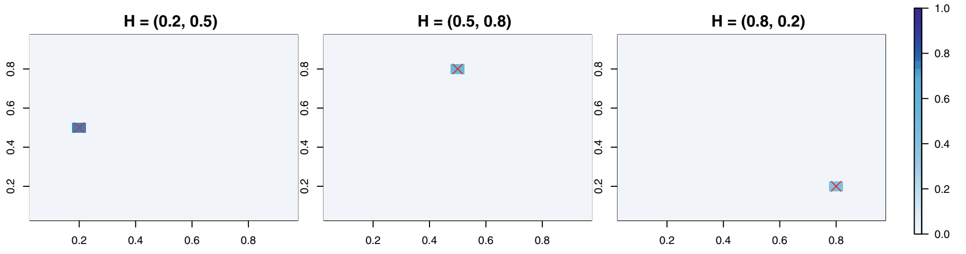

Figure 4. From *left* to *right*, the p values of the hypothesis test of (4) for fractional Brownian sheets with index $(0.2, 0.5)^T$, $(0.5, 0.8)^T$, and $(0.8, 0.2)^T$ are shown for $\mathbf{h} \in \mathcal{H} = \{j/20, j = 1, \ldots, 20\}^2$. Fractional Brownian sheets are generated at $\{(e^i, e^j), 1 \leq i, j \leq 20\}$. The true multi-self-similarity indexes are marked with *red crosses* (Color figure online).

Table 5. Self-similarity test for mixtures of fractional Brownian motions with index H and white noise, $X_H(t) + C\epsilon(t)$.

H	n	C			
		1	2	5	10
0.2	32	8.6 (.19)	11.6 (.19)	55.6 (.16)	94.0 (.14)
	64	7.6 (.20)	22.2 (.19)	88.2 (.16)	100 (.13)
	128	12.2 (.19)	71.2 (.18)	100 (.15)	100 (.12)
0.5	32	9.6 (.50)	8.8 (.50)	18.6 (.49)	51.0 (.47)
	64	7.8 (.50)	13.8 (.49)	47.8 (.48)	88.2 (.46)
	128	12.4 (.49)	48.4 (.48)	98.2 (.46)	100 (.44)
0.8	32	16.2 (.80)	17.0 (.80)	18.2 (.79)	32.0 (.78)
	64	10.8 (.80)	14.6 (.79)	42.6 (.78)	77.4 (.76)
	128	20.4 (.79)	67.8 (.78)	99.4 (.76)	100 (.74)

The empirical powers (%) of the test of (4) for $h = H$ are listed with the average centers of the intervals in the parentheses, calculated from 500 repetitions.

500 simulations for all n, H, and C, considered in this simulation study. We increase C and check if the self-similarity hypothesis is rejected. When $H = 0.2$, $n = 64$, and $C = 100$, the self-similarity hypothesis starts to be rejected, with higher frequency for larger C and larger n. If a fractional Brownian motion is dominated by white noise, which satisfies (1) for $H = 0$, the p value of the test of (4) is the largest when h is near zero. This implies that our test does not reject the self-similarity hypothesis when a self-similar process is contaminated by moderate amounts of measurement errors or random noise. However, the intervals of the estimated self-similarity indexes become biased downward as C increases. The average centers of the intervals of the estimated self-similarity indexes decrease as C increases in Table 5. Therefore, the percentages of the estimated intervals that exclude H, i.e., empirical powers (%) of the test of (4) for $h = H$, increase as C increases. The average lengths of the intervals of the estimated self-similarity indexes are not reported here as they are comparable to Table 1, regardless of the value of C. In summary, as the coefficient, C, or the sample size, n, increases, the more likely the interval of the estimated self-similarity indexes does not include the true index and the larger the downward bias in the interval of the estimated self-similarity indexes.

Table 6. The empirical powers (%) of the self-similarity test for Gaussian processes with generalized Cauchy covariance, $C(h) = (1 + |h|^{\alpha})^{-\beta/\alpha}$, $0 < \alpha \leq 2$, $\beta > 0$, observed at n locations of exponential index spacing, from 500 repetitions. The necessary condition for self-similarity holds if and only if $\alpha + \beta = 2$.

$(\alpha,\ \beta)$	n		
	32	64	128
(0.65, 1.35)	72.8	82.4	94.6
(1.95, 1.35)	75.2	84.0	95.2

Table 7. Subsequences of $\{1, \ldots, 2000\}$ that are on an exponential index spacing.

$\{[e^{i/9+m}], i = 19, \ldots, 68\}$
$\{[e^{i/10+m}], i = 20, \ldots, 76\}$
$\{[e^{i/11+m}], i = 30, \ldots, 83\}$
$\{[e^{i/12+m}], i = 35, \ldots, 91\}$
$\{[e^{i/13+m}], i = 40, \ldots, 98\}$

We consider 15 subsequences for $m = -0.1$, 0, and 0.1. The ranges of i differ slightly by m and those for $m = 0$ are given.

Finally, the generalized Cauchy family that can decouple the fractal dimension, D, and the Hurst parameter, H, was tested. The necessary condition for self-similarity is $D + H = d + 1$ (Gneiting and Schlather 2003). Even if the parameters of the generalized Cauchy and Dagum families are chosen to satisfy the condition, they are not self-similar in a strict sense as in our definition. The empirical powers of our test on the generalized Cauchy family are presented in Table 6. The empirical powers are comparable whether or not the linearity condition is met and comparable to the empirical powers of other non-self-similar processes shown in Tables 4 and 5.

3.2. STOCHASTIC PROCESS INDEXED IN ONE DIMENSION ON REGULAR INDEX SPACING

To test self-similarity of a process observed regularly in its domain, we simulate fractional Brownian motions with index $H = 0.2$, 0.5, and 0.8, at $t = 1, \ldots, 2000$, and sample a few subsequences of the process that are exponentially indexed as presented in Table 7. Table 8 shows the rejection rates of the self-similarity test, and the average centers and the average lengths of the intervals of the estimated self-similarity indexes, for all subsequences over all 500 simulations. The average lengths of the estimated intervals are much larger than those in Table 1, perhaps due to the rounding to a whole integer in sampling. Generally, the results vary by subsequence, indicating the need for multiple samplings.

To study empirical powers, we simulate time-deformed fractional Brownian motions, locally self-similar processes and mixtures of fractional Brownian motions and white noise considered in Tables 4 and 5, at $t = 1, \ldots, 2000$. Then, we test self-similarity of the subsequences in Table 7. Tables 9 and 10 show the rejection rates, the average centers, and

Table 8. Self-similarity test for the subsequences (in Table 7) of fractional Brownian motions with index H, for 500 times.

H	0.2	0.5	0.8
Rejection rate	3.8	0.0	14.6
Average center	0.23	0.51	0.75
Average length	0.34	0.36	0.33

The entries are the average rejection rates (%), the average centers, and the average lengths of the intervals of the estimated self-similarity indexes when the self-similarity hypothesis is not rejected.

Table 9. Self-similarity test for the subsequences (in Table 7) of time-deformed fractional Brownian motions and mean zero Gaussian processes with the Matérn covariance considered in Table 4.

$M(t)$	H		
	0.2	0.5	0.8
1.	14 (.20, .34)	2 (.36, .40)	2 (.55, .45)
2.	52 (.16, .30)	45 (.18, .31)	27 (.24, .33)
3.	26 (.18, .31)	8 (.23, .31)	3 (.23, .22)
4.	74 (.15, .29)	74 (.17, .27)	43 (.21, .26)
5.	35 (.17, .30)	17 (.18, .27)	14 (.15, .20)
6.	54 (.16, .30)	46 (.16, .31)	36 (.17, .32)
7.	21 (.18, .31)	2 (.25, .33)	0 (.35, .32)

The average rejection rates (%) from 500 repetitions are listed along with the average centers and the average lengths of the intervals of the estimated self-similarity indexes in the parentheses, when the self-similarity hypothesis is not rejected.

Table 10. Self-similarity test for the subsequences (in Table 7) of mixtures of fractional Brownian motion with index H and white noise, $X_H(t) + C\epsilon(t)$.

	H	C			
		1	2	5	10
Rejection rate (empirical powers)	0.2	11 (14.0)	22 (30.9)	45 (55.5)	53 (62.6)
	0.5	0 (19.2)	0 (45.6)	2 (89.2)	9 (98.5)
	0.8	6 (28.6)	2 (54.1)	0 (93.0)	0 (99.4)
(center, length)	0.2	(.19, .32)	(.16, .29)	(.14, .27)	(.14, .27)
	0.5	(.45, .36)	(.38, .35)	(.26, .33)	(.19, .30)
	0.8	(.72, .33)	(.66, .33)	(.53, .33)	(.42, .32)

In the top half, the average rejection rates (%) from 500 repetitions are listed along with the percentages of the intervals of the estimated self-similarity indexes that exclude H (empirical powers (%) of the test of (4) for $h = H$) in the parentheses. In the bottom half, the average centers and the average lengths of the estimated intervals are listed.

the average lengths of the estimated intervals when self-similarity is not rejected. The trends in the rejection rates and the estimated indexes are similar to the case of exponential index spacing presented in Tables 4 and 5.

Most existing tests do not have a formal criterion for the acceptance of self-similarity except Bianchi (2004), who proposed to test self-similarity based on a Kolmogorov–Smirnov

Table 11. The empirical sizes of the proposed test and Bianchi's test applied to 200 fBMs with index H, observed at 2000 regular index spacing. The test is conducted at a significance level of $\alpha = 0.05$.

Proposed test	H	0.30	0.40	0.50	0.60	0.70
	Empirical size	0.010	0.045	0.050	0.050	0.080
Bianchi's test	H	0.30	0.40	0.50	0.60	0.70
	Empirical size	0.005	0.050	0.050	0.050	0.035

goodness-of-fit test. Although we were not able to carry out an apple-to-apple comparison, we conducted the same simulation study that was considered in Bianchi (2004, Table 1): 200 fBMs observed on a regular index spacing of size $n = 2000$. We used the subsequences in Table 7. For fair comparison, we rejected the null hypothesis, H-ss, if the estimated interval for self-similarity index excluded H. The empirical sizes were compared in Table 11, and both tests produced comparable results. Bianchi's test was applied to multifractional Brownian motions and uniform random walks to study empirical powers. However, it did not reject self-similarity in all simulations. Our proposed test had better empirical powers when detecting non-self-similarity of time-deformed fBMs.

3.3. Random Fields Indexed in Two Dimensions

The fractional Brownian sheet is a generalization of the fractional Brownian motion to higher dimensions. There are two definitions of the fractional Brownian sheet (Genton et al. 2007). Both are mean zero Gaussian processes. Under the first definition, the fractional Brownian sheet with index $H \in (0, 1]$, X_H, satisfies, for all $\mathbf{t} = (t_1, \ldots, t_d)^T$ and $\mathbf{s} = (s_1, \ldots, s_d)^T \in \mathbb{R}^d$,

$$\mathrm{E}\{X_H(\mathbf{t})X_H(\mathbf{s})\} = \frac{1}{2^d}\left(\|\mathbf{t}\|^{2H} + \|\mathbf{s}\|^{2H} - \|\mathbf{t}-\mathbf{s}\|^{2H}\right). \tag{7}$$

Then, the fractional Brownian sheet is H-ss or $\mathbf{H}$-mss for $\mathbf{H} = (H, \ldots, H)^T/d$. Under the second definition, $X_{\mathbf{H}}$ follows the fractional Brownian sheet with index $\mathbf{H} = (H_1, \ldots, H_d)^T \in (0, 1]^d$, if it satisfies, for all $\mathbf{t}$ and $\mathbf{s} \in \mathbb{R}^d$,

$$\mathrm{E}\{X_{\mathbf{H}}(\mathbf{t})X_{\mathbf{H}}(\mathbf{s})\} = \frac{1}{2^d}\prod_{i=1}^{d}\left(|t_i|^{2H_i} + |s_i|^{2H_i} - |t_i - s_i|^{2H_i}\right). \tag{8}$$

Then, $X_{\mathbf{H}}$ is $\mathbf{H}$-mss.

We simulate fractional Brownian sheets with index $\mathbf{H} = (0.2, 0.5)^T$, $(0.5, 0.8)^T$, and $(0.8, 0.2)^T$, $\{X_{\mathbf{H}}(e^i, e^j),\ i, j = 1, \ldots, 20\}$ and their mixtures with white noise. Figure 4 shows the p values of the stationarity test for $Y_{\mathbf{h}}, \mathbf{h} \in \mathcal{H} = \{j/20,\ j = 1, \ldots, 20\}^2$, for a realization of the fractional Brownian sheet with index $(0.2, 0.5)^T$, $(0.5, 0.8)^T$, and $(0.8, 0.2)^T$, from left to right. The p values of the stationarity test for $Y_{\mathbf{h}}$ are positive only at the true index. Table 12 lists the rejection rates of the multi-self-similarity test along with the average centers and the average diameters of the set of the estimated indexes when the multi-self-similarity hypothesis is not rejected. The average centers and diameters indicate

Table 12. Multi-self-similarity test for the mixtures of the fractional Brownian sheets and white noise, $\{X_{\mathbf{H}}(\mathbf{t}) + C\epsilon(\mathbf{t}), \mathbf{t} = (e^i, e^j), i, j, = 1, \ldots, 20\}$, for 100 times, for $\mathcal{H} = \{j/20, j = 1, \ldots, 20\}^2$.

H		C		
		0	2	5
$(0.2, 0.5)^T$	Rejection rate	14	27	24
	Average center	(.201, .501)	(.200, .500)	(.199, .497)
	Average diameter	0.05	0.05	0.05
$(0.5, 0.8)^T$	Rejection rate	13	26	24
	Average center	(.502, .801)	(.502, .801)	(.497, .800)
	Average diameter	0.05	0.05	0.05
$(0.8, 0.2)^T$	Rejection rate	31	29	24
	Average center	(.800, 0.202)	(0.800, 0.201)	(0.798, 0.199)
	Average diameter	0.05	0.05	0.05

The entries are the rejection rates (%) of the multi-self-similarity test, the average centers, and the average diameters of the set of the estimated multi-self-similarity indexes.

that the multi-self-similarity index is estimated accurately when the multi-self-similarity hypothesis is not rejected.

4. APPLICATIONS

In the real applications we consider in this section, we assume that the underlying stochastic process has stationary increments. In practice, the origin of the observed process is arbitrary or unclear. If X is multi-self-similar, $X(\mathbf{t}) \to 0$ as $\|\mathbf{t} - \mathbf{0}\| \to 0$ in probability, by letting $a_1, \ldots, a_d$ converge to zero in (2). Therefore, instead of testing multi-self-similarity of the observed process, we test multi-self-similarity of the difference from a reference point. For example, suppose that we observe a process, X, on a regular grid of size $n_1 \times \cdots \times n_d$, for some $n_1, \ldots, n_d \in \mathbb{N}$. We test if the difference of X at the grid points $(i_1, \ldots, i_d)$ and $(1, \ldots, 1)$ is a multi-self-similar process observed at $\{(i_1 - 1, \ldots, i_d - 1), \; i_j = 1, \ldots, n_j, \; j = 1, \ldots, d\}$, which is true if X is multi-self-similar and has stationary increments, i.e., $X(\mathbf{t}) - X(\mathbf{s}) \stackrel{\mathcal{L}}{=} X(\mathbf{t} - \mathbf{s})$ for all $\mathbf{t}$ and $\mathbf{s} \in \mathbb{R}^d$.

4.1. NILE RIVER DATA

Annual minimum water levels of the Nile River are known to be long-range dependent, also known as the Joseph effect, which describes persistence over time. The series is examined in a number of papers and well modeled by a fractional Gaussian noise (fGn) process, a stationary long-memory process that arises as increments of fractional Brownian motion with parameter H. Bardet (2000) concluded that the yearly lowest water levels between year 722 and 1281 follow fGn processes with $H \approx 0.88$. The data are available to download at the machine learning dataset repository (http://mldata.org/repository/data/viewslug/nile-water-level/).

We draw 15 subsequences from the cumulative summation of the Nile River data, each of which consists of around 40 data values. For all subsequences, the self-similarity test with

Table 13. Intervals of the estimated self-similarity indexes of the annual minimum water levels of the Nile River, by subsequences.

	m		
	0	0.1	−0.1
$X([e^{i/9+m}]),\ i = 19, \dots, 58$	(.79, .99)	(.80, .99)	(.81, .99)
$X([e^{i/10+m}]),\ i = 20, \dots, 65$	(.82, .99)	(.81, .99)	(.82, .99)
$X([e^{i/11+m}]),\ i = 30, \dots, 71$	(.77, .99)	(.78, .99)	(.79, .99)
$X([e^{i/12+m}]),\ i = 37, \dots, 77$	(.76, .99)	(.75, .99)	(.79, .99)
$X([e^{i/13+m}]),\ i = 40, \dots, 84$	(.78, .99)	(.75, .99)	(.77, .99)

The ranges of i differ slightly by m, and those for $m = 0$ are given.

$\mathcal{H} = \{j/100,\ j = 1, \dots, 100\}$ concludes that the annual minimum water levels of the Nile River are H-ss for some $H \in (0.76, 1)$. Table 13 shows the subsequences and the intervals of the estimated self-similarity indexes. All estimated intervals include $(0.83, 0.88)$, the range of the estimated H of the Nile River data in the literature.

4.2. NETWORK TRAFFIC DATA

We analyze two LAN traffic traces, each of which contains a million packet arrivals seen on an Ethernet at the Bellcore Morristown Research and Engineering facility. One trace began at 11:25 a.m. on August 29, 1989, and ran for 3142.82 s, the other began at 11:00 a.m. on October 5, 1989, and ran for 1759.62 s. They are subsets of the traffic data analyzed by Leland et al. (1994), in which the self-similarity index of the network traffic is estimated separately for busy, normal, or idle periods. The estimated self-similarity indexes in Leland et al. (1994) ranged from 0.75 to 0.95, with higher indexes for busy periods in general. The traces are downloadable from the Internet Traffic Archive sponsored by the Association for Computing Machinery's Special Interest Group on Data Communications (ACM SIGCOMM, http://ita.ee.lbl.gov/html/contrib/BC.html). The traces consist of two variables: time in seconds since the start of the trace that are accurate to 10 microseconds and the Ethernet data length in bytes, not including the Ethernet preamble, header, or CRC (cyclic redundancy check). The Ethernet protocol forces all packets to have at least the minimum size of 64 bytes and at most the maximum size of 1518 bytes.

By definition, the self-similarity index is not affected by the rescaling of the process by time. We aggregate the arrived data amounts by 2, 5, and 10 s as in Leland et al. (1994). Let $X(i-1)$ be the difference in the Ethernet traffic amounts (kilobytes) between the ith and the first time unit. Figure 5 shows $\{X(i), i = 0, \dots, n-1\}$ by trace and aggregation level, for $n = 300$ (*left*) and 150 (*right*).

We test self-similarity of the 15 subsequences listed in Table 14, with $\mathcal{H} = \{j/100,\ j = 1, \dots, 100\}$. For each aggregation level, at most one subsequence rejects the self-similarity hypothesis and all the others conclude that the LAN traffic amount is self-similar with some index, $h \in (0, 1]$. Table 15 lists the rejection rates of the self-similarity hypothesis, the average centers and the average lengths of the intervals of the estimated self-similarity indexes, the average lengths of the subsequences, and the lengths of the aggregated traces by aggregation level. The estimated self-similarity index increases as we increase the time

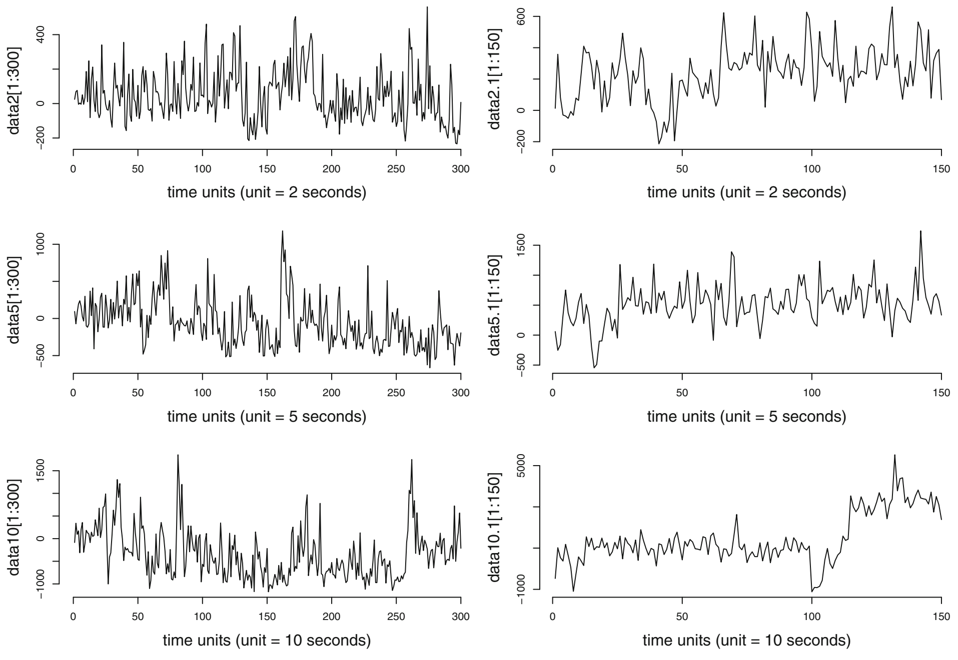

Figure 5. Differences in the Ethernet traffic amounts (kilobytes per time unit) of the first 300 (*left*) and 150 (*right*) time units from that of the first time unit. The Ethernet traffic traces are from the Bellcore Morristown Network on August 29, 1989 (*left*) and October 5, 1989 (*right*) on three different time scales.

Table 14. Subsequences of LAN traffic traces selected for the self-similarity test, for $m = -0.3$, 0, and 0.5.

$\{[e^{i/5+m}]), i = 9, \ldots, 38\}$
$\{[e^{i/10+m}]), i = 24, \ldots, 75\}$
$\{[e^{i/15+m}]), i = 50, \ldots, 112\}$
$\{[e^{i/20+m}]), i = 80, \ldots, 149\}$
$\{[e^{i/30+m}]), i = 130, \ldots, 222\}$

The end point varies by $m = -0.3$, 0, and 0.5. The ranges of i differ by m and the length of the level of time aggregation of the traces. The ranges of i for $m = 0$ for the trace on August 29, aggregated by 2 s, are given.

Table 15. Self-similarity test for the subsequences (Table 14) of the LAN traffic traces seen at the Bellcore Morristown Network.

Data aggregate by (s)	Aug. 29			Oct. 5		
	2	5	10	2	5	10
Rejection (out of 15)	1	0	0	0	0	1
Average center	0.08	0.19	0.33	0.24	0.43	0.57
Average length	0.12	0.35	0.57	0.37	0.46	0.49
Average length of subsequence	100	73	52	83	55	34
Length of trace	1571	628	314	879	351	175

scale by which the amount of network traffic is aggregated. We suspect that when the time aggregation is large, the effect of random noise in the LAN traffic traces is relatively reduced. Therefore, the intervals of the estimated self-similarity indexes include the estimates by

Leland et al. (1994) when the time aggregation level is high. For example, when aggregated by 10 s, four and ten subsequences have the interval of the estimated self-similarity indexes that include 0.75 for August 29 and October 5, respectively. The large estimated interval of the self-similarity indexes for high aggregation levels is associated with decreases in the lengths of the traces and the subsequences.

4.3. SPATIAL DATA: FOOD WRAP

The heights of the surfaces of plastic food wrappings were measured at the atomic level by a scanning tunneling electron microscope. The data were collected and analyzed in an effort to produce smooth wrappings to which it would be difficult for microorganisms to adhere. Davies and Hall (1999) described details of the data, which consisted of 128×128 grid observations that measured height averages close to grid point centers. The pixels were 40 nm $\times$ 40 nm and six food wrappings were examined. Let $X(i, j)$ be the difference in the surface heights at $(i+1, j+1)$ and $(1, 1)$, for $i, j = 0, \ldots, 127$. Figure 6 shows the image plots of X for the six food wrappings, (a–f).

We select sixteen subsequences, $\{X(t_{i,k}, t_{j,l})\}_{k,l}$, for $i, j = 1, \ldots, 4$, by combining four subsequences of $\{0, \ldots, 127\}$ presented in Table 16. Table 17 shows the results of the multi-self-similarity test with $\mathcal{H} = \{i/20,\ i = 1, \ldots, 20\}^2$. It lists the number of the cases that reject the multi-self-similarity hypothesis out of 16 subsequences. Also listed are the average centers and the average diameters of the set of the estimated multi-self-similarity indexes that are averaged over the subsequences that do not reject the multi-self-similarity hypothesis. All the 16 subsequences of wrapping (c) reject the multi-self-similarity hypothesis, therefore the information on the set of the estimated indexes is not available (n/a). The rejection rates are high except for wrappings (b) and (f), which indicates that the anisotropic modeling in Davies and Hall (1999) might be a solution for this. Davies and Hall (1999) modeled the food wrappings as anisotropic asymptotically self-similar processes:

$$\log[\mathrm{E}\{X(\mathbf{t}) - X(\mathbf{0})\}^2] = c + H\log(1 + s\cos[2\{\arg(\mathbf{t}) - \psi\}]) + 2H\log(\|\mathbf{t}\|), \quad (9)$$

as $\|\mathbf{t} - \mathbf{0}\| \to 0$, for $c \in \mathbb{R}$ and $\psi \in (0, 2\pi]$, where s is the strength of anisotropy and $\arg(\mathbf{t})$ is the angle made by the vector $\mathbf{t}$ to a fixed direction in the plane. A H-ss process satisfies (9) for all $\mathbf{t} \in \mathbb{R}^d$ with $s = 0$. Davies and Hall (1999, Table 1) estimated H under (9), and found that they were 0.5, 0.51, 0.70, 0.81, 0.53, and 0.41 for the wrappings (a–f), respectively. According to Table 17, 7 and 14 subsequences do not reject the multi-self-similarity hypothesis for wrappings (a) and (f), respectively. Among those, 3 and 9 subsequences had the set of the estimated indexes that included $(0.5, 0.5)/2$ and $(0.41, 0.41)/2$, respectively. According to Table 17, wrappings (b) and (e) seem to follow a multifractal process rather than a self-similar process with a common self-similarity index for all of its coordinates, which might explain the exclusion of $(0.51, 0.51)/2$ and $(0.53, 0.53)/2$ from the set of the estimated indexes of all subsequences that did not reject the multi-self-similarity hypothesis. In conclusion, we see that for anisotropic processes such as the processes in Fig. 6, the multi-self-similarity hypothesis is often rejected. And when it is not rejected, our approach estimates the multi-self-similarity index under anisotropy correctly.

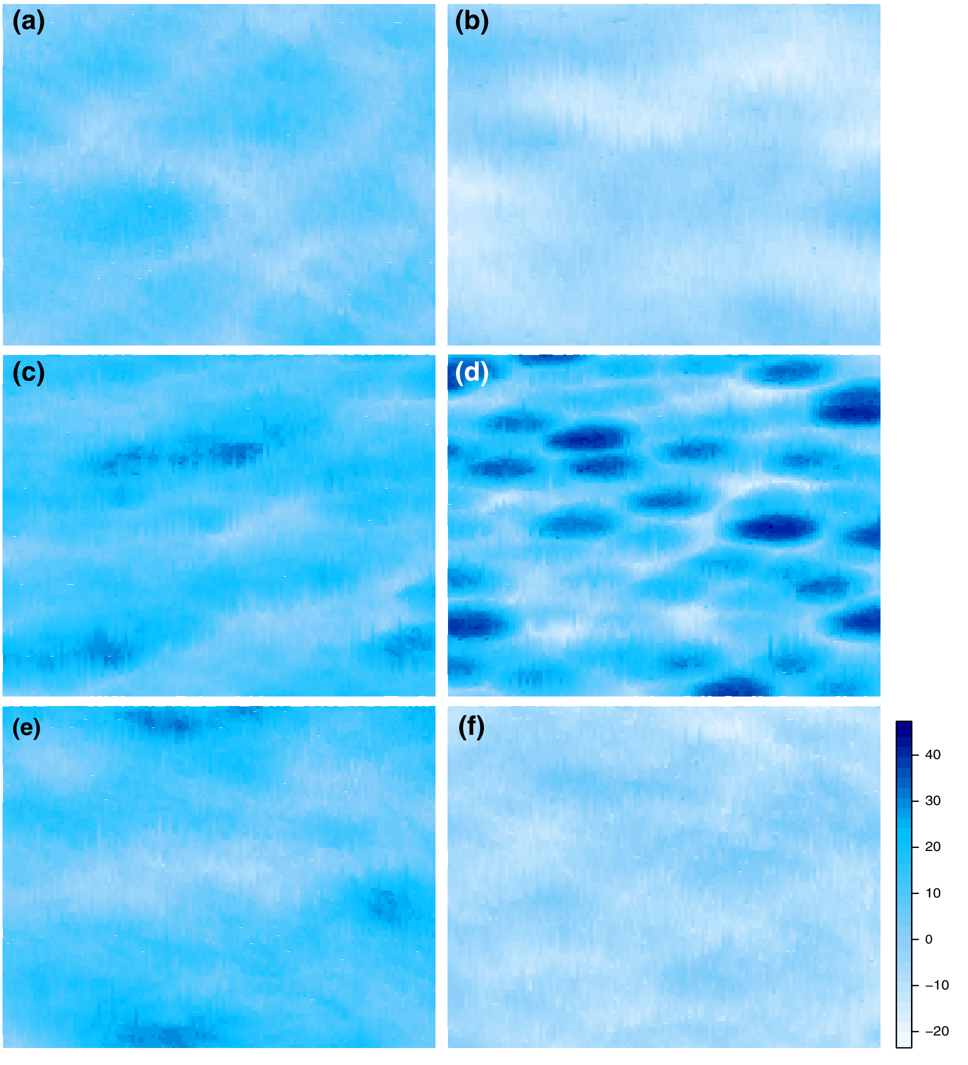

Figure 6. Differences in the surface heights of the food wrappings from that of the first grid point.

Table 16. Subsequences of $\{0, \ldots, 127\}$ selected for the multi-self-similarity test for the food wrapping data.

$\{t_{1,k} = [e^{k/12}],\ k = 31, \ldots, 58\}$
$\{t_{2,k} = [e^{k/16}],\ k = 45, \ldots, 77\}$
$\{t_{3,k} = [e^{k/20}],\ k = 58, \ldots, 97\}$
$\{t_{4,k} = [e^{k/21}],\ k = 60, \ldots, 101\}$

Table 17. Multi-self-similarity test for the wrappings in Fig. 6.

Food wrapping	(a)	(b)	(c)	(d)	(e)	(f)
Rejection (out of 16)	9	4	16	15	10	2
Average center	(0.20, 0.29)	(0.10, 0.53)	n/a	(0.05, 0.06)	(0.11, 0.83)	(0.19, 0.19)
Average diameter	0.19	0.25	n/a	0.08	0.19	0.23

5. DISCUSSION

We developed a statistical hypothesis test for multi-self-similarity of a stochastic process using the Lamperti transformation and stationarity tests (Priestley and Subba Rao 1969; Fuentes 2005). If the multi-self-similarity hypothesis of the process is not rejected, we provide a set of the estimated multi-self-similarity indexes. The empirical sizes and powers were studied for various stochastic processes and the test was applied to several real datasets. The multi-self-similarity test that we propose correctly accepts multi-self-similarity of fractional Brownian motions and sheets most of the time. It does not reject the multi-self-similarity hypothesis when a multi-self-similar process is corrupted by moderate size of random noise. We report the power of the test on time-deformed self-similar processes, locally self-similar processes, and anisotropic processes.

There are many stationarity tests for a stochastic process in one dimension. Some of them aim to detect the region of the series where non-stationarity occurs and test for local stationarity (Nason 2013). Intuitively, a locally stationary process behaves approximately stationary over short periods of time. By testing several subsequences of the process, we can extend this paper to detect the part of the process in which non-multi-self-similarity occurs. Also, testing asymptotic self-similarity is left for future research.

ACKNOWLEDGEMENTS

This work was partially supported by NSF Grant DMS-1208421 and Award No. KUS-C1-016-04 made by King Abdullah University of Science and Technology (KAUST).

[Received September 2015. Accepted June 2016. Published Online July 2016.]

APPENDIX: DETAILS OF TESTING PROCEDURE

For the stationarity test for $\{Y_{\mathbf{h}}(\mathbf{u}), \mathbf{u} = (u_1, u_2)^T, u_1 = 1, \ldots, n_1, u_2 = 1, \ldots, n_2\}$, we select locations, $\mathbf{t}_1 = ([n_1/4], [n_2/4])^T$, $\mathbf{t}_2 = (3[n_1/4], [n_2/4])^T$, $\mathbf{t}_3 = ([n_1/4], 3[n_2/4])^T$, and $\mathbf{t}_4 = 3\mathbf{t}_1$, and frequencies, $\boldsymbol{\omega}_1 = (\pi/4, \pi/4)^T$ and $\boldsymbol{\omega}_2 = 3\boldsymbol{\omega}_1$. Following the notation of Fuentes (2005), the estimate of the evolutionary spectral density function at location $\mathbf{t} \in \mathbb{R}^2$ at frequency $\boldsymbol{\omega} \in (-\pi, \pi)^2$ is

$$\hat{f}_{\mathbf{t}}(\boldsymbol{\omega}) = \int_{-\infty}^{\infty}\int_{-\infty}^{\infty} W_\rho(\mathbf{t}-\mathbf{s})|J_{\mathbf{s}}(\boldsymbol{\omega})|^2 d\mathbf{s}, \tag{10}$$

where $\mathbf{s} = (s_1, s_2)^T \in \mathbb{R}^2$ and $W_\rho(\mathbf{s}) = I(-\rho/2 \le s_1, s_2 \le \rho/2)/\rho^2$. The indicator function, $I(x \in A)$, equals one if $x \in A$ and zero otherwise. The tapered spatial periodogram is

$$J_{\mathbf{s}}(\boldsymbol{\omega}) = \sum_{u_1=0}^{n_1}\sum_{u_2=0}^{n_2} g(\mathbf{s}-\mathbf{u})Y_{\mathbf{h}}(\mathbf{u}) \exp\{-i\mathbf{u}^T\boldsymbol{\omega}\}, \tag{11}$$

for $\mathbf{u} = (u_1, u_2)^T$ and $g(\mathbf{s}) = I(-h \le s_1, s_2 \le h)/(4h\pi)$. The evolutionary spectrum is estimated by smoothing the spatial periodograms within the region of window ρ and frequencies of window π/h. We select the windows, $\rho = (n_1 \wedge n_2)/2$ and $h = 2$, so that the spacing between $\{\mathbf{t}_1, \ldots, \mathbf{t}_4\}$ and $\{\boldsymbol{\omega}_1, \boldsymbol{\omega}_2\}$ is at least the size of the windows, respectively. The integration in (10) is approximated by Monte Carlo integration by generating a random number $\mathbf{s}$ such that $W_\rho(\mathbf{t}_i - \mathbf{s}) > 0$, for each i, for 500 times. We drop the second coordinates of $\mathbf{t}_i$ and $\boldsymbol{\omega}_j$ for a stochastic process indexed in one dimension.

Let $f_{\mathbf{t}}(\boldsymbol{\omega})$ be the spatial spectral density of $Y_{\mathbf{h}}$. Under the conditions of Fuentes (2005, theorem 1), $\log\{\hat{f}_{\mathbf{t}_i}(\boldsymbol{\omega}_j)\}$ is asymptotically normal with mean $\log\{f_{\mathbf{t}_i}(\boldsymbol{\omega}_j)\}$, variance $\sigma^2 = 16h^2/\rho^2$, and zero covariance for all i and j. We test stationarity of $Y_{\mathbf{h}}$ by testing $H_0 : \alpha_1 = \alpha_2 = \alpha_3 = \alpha_4$ vs H_a : not H_0, in the following linear model:

$$\log\{\hat{f}_{\mathbf{t}_i}(\boldsymbol{\omega}_j)\} = \mu + \alpha_i + \epsilon_{ij},$$

where μ is a grand mean, $\sum_i \alpha_i = 0$, and ϵ_{ij} follow iid normal distributions with mean zero and variance σ^2 for all i and j. The sum of squares between locations, $2\sum_i(\hat{\mu} - \hat{\alpha}_i)^2/\sigma^2$, follows a χ^2_3 under H_0, in two dimensions (χ^2_1 in one dimension), where $\hat{\mu}$ is the sample mean of $\log\{\hat{f}_{\mathbf{t}_i}(\boldsymbol{\omega}_j)\}$ and $\hat{\alpha}_i = \sum_j \log\{\hat{f}_{\mathbf{t}_i}(\boldsymbol{\omega}_j)\}/2$.

REFERENCES

Bai, X. and Shami, A. (2013), "Modeling Self-similar Traffic for Network Simulation," Available at http://arxiv.org/pdf/1308.3842.pdf.

Bardet, J.-M. (2000), "Testing for the Presence of Self-Similarity of Gaussian Time Series Having Stationary Increments," *Journal of Time Series Analysis*, 21, 497–515.

Bianchi, S. (2004), "A New Distribution-based Test of Self-Similarity," *Fractals-Complex Geometry Patterns and Scaling in Nature and Society*, 12, 331-346.

Cardinali, A. and Nason, G. P. (2011), "Costationarity of Locally Stationary Time Series," *Journal of Time Series Econometrics*, 2, 1–35.

Davies, S. and Hall, P. (1999), "Fractal Analysis of Surface Roughness by Using Spatial Data. (With discussion)." *Journal of the Royal Statistical Society Series B*, 61, 3–37.

Dwivedi, Y. and Subba Rao, S. (2011), "A Test for Second-order Stationarity of a Time Series Based on the Discrete Fourier Transform," *Journal of Time Series Analysis*, 32, 68–91.

Flandrin, P., Borgnat, P., and Amblard, P.-O. (2003), "From Stationarity to Self-similarity, and Back: Variations on the Lamperti Transformation," in *Processes with Long-Range Correlations*, eds. Rangarajan, G. and Ding, M., Springer Berlin Heidelberg, vol. 621 of *Lecture Notes in Physics*, pp. 88–117.

Fuentes, M. (2005), "A Formal Test for Nonstationarity of Spatial Stochastic Processes," *Journal of Multivariate Analysis*, 96, 30–54.

Genton, M. G., Perrin, O., and Taqqu, M. S. (2007), "Self-Similarity and Lamperti Transformation for Random Fields," *Stochastic Models*, 23, 397–411.

Ghanbarian-Alavijeh, B., Millán, H., and Huang, G. (2011), "A Review of Fractal, Prefractal and Pore-solid-fractal Models for Parameterizing the Soil Water Retention Curve," *Canadian Journal of Soil Science*, 91, 1–14.

Gneiting, T., Ševčíková, H., and Percival, D. B. (2012), "Estimators of Fractal Dimension: Assessing the Smoothness of Time Series and Spatial Data," *Statistical Science*, 27, 247–277.

Gneiting, T. and Schlather, M. (2003), "Stochastic Models That Separate Fractal Dimension and Hurst Effect," *SIAM Review*, 46, 269–282.

Hall, P., Härdle, W., Kleinow, T., and Schmidt, P. (2000), "Semiparametric Bootstrap Approach to Hypothesis Tests and Confidence Intervals for the Hurst Coefficient," *Statistical Inference for Stochastic Processes*, 3, 263–276.

Jentsch, C. and Subba Rao, S. (2015), "A Test for Second Order Stationarity of a Multivariate Time Series," *Journal of Econometrics*, 185, 124-161.

Jun, M. and Genton, M. G. (2012), "A Test for Stationarity of Spatio-Temporal Random Fields on Planar and Spherical Domains," *Statistica Sinica*, 22, 1737–1764.

Kent, J. T. and Wood, A. T. A. (1997), "Estimating the Fractal Dimension of a Locally Self-similar Gaussian Process by Using Increments," *Journal of the Royal Statistical Society Series B*, 59, 679–699.

Lamperti, J. (1962), "Semi-stable Stochastic Processes," *Transactions of the American Mathematical Society*, 104, 62–78.

Leland, W. E., Taqqu, M. S., Willinger, W., and Wilson, D. V. (1994), "On the Self-similar Nature of Ethernet Traffic (extended version)," *IEEE/ACM Transactions on Networking*, 2, 1–15.

Li, M. and Zhao, W. (2012), "Quantitatively Investigating the Locally Weak Stationarity of Modified Multifractional Gaussian Noise," *Physica A: Statistical Mechanics and its Applications*, 391, 6268–6278.

Nason, G. (2013), "A Test for Second-order Stationarity and Approximate Confidence Intervals for Localized Autocovariances for Locally Stationary Time Series," *Journal of the Royal Statistical Society Series B*, 75, 879–904.

Priestley, M. B. and Subba Rao, T. (1969), "A Test for Non-stationarity of Time-series," *Journal of the Royal Statistical Society Series B*, 31, 140–149.

Samorodnitsky, G. and Taqqu, M. S. (1994), *Stable Non-Gaussian Random Processes: Stochastic Models with Infinite Variance*, New York: Chapman & Hall.

Stein, M. L. (1999), *Interpolation of Spatial Data. Some Theory for Kriging.*, New York: Springer.

Subba Rao, S. (2008), "Statistical Analysis of a Spatio-Temporal Model with Location-Dependent Parameters and a Test for Spatial Stationarity," *Journal of Time Series Analysis*, 29, 673–694.

Wang, Y., Cavanaugh, J. E., and Song, C. (2001), "Self-Similarity Index Estimation via Wavelets for Locally Self-Similar Processes," *Journal of Statistical Planning and Inference*, 99, 91–110.